Desalination and Water Treatment
www.deswater.com

doi: 10.5004/dwt.2021.26691

213 (2021) 406–417
February

Synthesis of eco-friendly alginate-based supports for silver oxide immobilization in catalytic degradation of textile dyes

Azeem Bibi[a], Sadiq-ur-Rehman[a,*], Tasleem Akhtar[b], Ikhtiar Ahmad[a]

[a]*Department of Chemistry, University of Azad Jammu and Kashmir, Muzaffarabad, Pakistan, Tel. +92 3018086819; emails: srkhattak@gmail.com (Sadiq-ur-Rehman), azeembibi786@gmail.com (A. Bibi), ikhtiarahmad@gmail.com (I. Ahmad)*
[b]*Department of Zoology, University of Azad Jammu and Kashmir, Muzaffarabad, Pakistan, email: seemeawan88@gmail.com*

Received 9 February 2020; Accepted 7 October 2020

ABSTRACT

Significant efforts were done to prepare eco-friendly supports for the immobilization of silver oxide nanoparticles. Alginate was interacted with chitosan in the presence of functionalized multi-walled carbon nanotubes (COOH-MWCNTs) under ultrasonic waves to form polymeric nanocomposite supports. Silver oxide nanoparticles were made to embed and react with polymeric supports in the presence of surfactants to form nanocomposite catalysts (Cs90 (Ag_2O), Cc90 (Ag_2O), CD90 (Ag_2O)). Advanced instrumental techniques such as scanning electron microscopy (SEM), transmission electron microscopy (TEM), Fourier transform infrared spectroscopy (FTIR), UV-visible spectrophotometry (UV), X-rays diffractometry and Brunauer–Emmett–Teller (BET) analysis were used to characterize the nanoparticles as well as nanocomposites. The nanoparticles were uniformly dispersed and embedded in the alginate-based supports, indicated by SEM and TEM. The physicochemical interactions between nanoparticles and matrix were indicated by FTIR spectroscopy. More surface area of newly formulated catalysts compared with pristine polymers is shown by the BET technique. The porous nature made the catalysts to show the best results in the degradation of methylene blue (MB), methyl orange (MO) and eosin Y (EY) by providing reactive centers and diffusion pathways. It is known that prepared nanocomposites have potential to use as catalysts for many times, suggesting their inclusion in the water flow system.

Keywords: Alginate–chitosan; Supporting matrix; Immobilization; Degradation of dyes; Catalysts

1. Introduction

In the modern period of science and technology, the role of industries in development related to new and huge mass synthesis is very common. But unfortunately, this development is pervasively connected with the disposal of many hazardous pollutants. Synthetic dyes are the result of these industrial developments that have various forms (more than 100,000 individual dyes are produced) and are widely used in textile, paper, leather tanning, food processing, plastics, cosmetics, rubber, and dye printing industries [1]. In up-to-date data, 7×10^5 tons of dyes are produced per year and 2% of them are discharged into rivers, oceans, lakes, and in other water resources [2]. The World Bank estimated that 72 toxic chemicals are included in water bodies from dyestuff in which 30 are not removed [3]. Various environmental and health problems such as cancer, splenic sarcoma, cytoplasmic anomalies and allergic problems along with the bad effect on water quality, photosynthesis, soil productivity are related to dye substances [4–7]. So, for human health and environmental safety,

* Corresponding author.

it is the utmost need to remove dyestuff from water bodies. During past decades various methods have been practiced removing dye pollutants. The most commonly used ones are oxidative processes, biodegradation, adsorption, incineration, solvent extraction, distillation, etc. But these methods are less efficient, costly, critical, and time-consuming [8].

Catalytic degradation is a practical remediation technology that is widely used due toclean, easy, and rapid process. In this method, dyes are degraded into simple molecules in the presence of suitable catalysts. But problems such as low separation, recycling and deformation of catalysts hinder its widespread acceptance. The above problems can be overcome by the immobilization of catalysts on some supports. The immobilization is a unique way in industrial catalysis, as it enhances the recovery and recycling of a catalyst along with its greater reactive sites and promising action (chemo and stereo-selectivity, stability and diffusional action) [9]. Various materials have been developed to be used as supporting materials for immobilization of catalysts, for example, glass beads, stainless steel, aluminum, metal alloys, ash-based materials, clay-based materials, etc. [10–13].

However, the current quest is for cleaner, biodegradable, and sustainable materials that reduce the environmental impact due to their disposal after use [14]. The applications of hydrocarbons as a supporting matrix for immobilization of catalytic particles are suggested to more efficient due to large bonding potential for metal ions by complexation, chelation, and ion exchange mechanisms [15–17].

Alginate is a natural anionic polysaccharide obtained from brown seaweed and consists of β-D-mannuronic acid and its C_5-epimer α-L-guluronic acid linked via β-1,4-glycosidic bonds [18]. It is biodegradable, sustainable and largely investigated for immobilization of catalytic particles due to plentiful –OH and –COOH functional groups in its backbone [19]. Similarly, chitosan is a cationic polysaccharide and consists of glucosamine and acetyl-glucosamine units. It is also a biodegradable polymer and has the potential to provide sustainable and insoluble support to catalyst [20,15]. These polymers are very efficient for acting as supporting materials and provide more reacting sites to catalyze a reaction. However, their pristine forms cannot be used in recycling turns (as alginate, similar to other polysaccharides, is fragile, highly swelled and disintegrates easily) and leach out in reaction systems [21,22].

To overcome the persisting problems such as leaching, disintegration, water solubility, and utilizing the potential aptitudes to immobilize the metallic oxide particles, an emerging field of nanotechnology was applied. It is known that the role of nanotechnology and nanoparticles are very appreciating to improve the strength, surface area and other physico-chemical properties of natural polymers [23]. Carbon nanotubes (CNTs) are the nanoparticles that act as best reinforcing materials and have a large surface area, greater chemical reactivity, high aspect ratio, less chemical mass and greater strength [24–26]. A large number of documents are filed in literature in which CNTs react physio-chemically with –OH and –COOH functional groups of alginate and chitosan and formed nanocomposite scaffolds with promising properties [27,28,15]. Adding CNTs to alginate as well as in the chitosan matrix, the thermo-mechanical properties and surface area of polymers increased. Moreover, it is known that embedded CNTs in polymeric matrix enhance the surface area to coordinate the catalyst by coordinating substrate molecules through a range of noncovalent bonding interactions [15,29].

Based on this work, the current study aims to formulate new supporting matrices that would be more stable, insoluble, porous and provide more reactive centers for catalytic action. For such purpose, alginate was interacted with chitosan in the presence of COOH-MWCNTs and surfactants under ultrasonic waves. The metallic oxide particles (Ag_2O) were immobilized in algi+chito/CNTs matrix by sonication to form catalysts (Cs90 (Ag_2O), Cc90 (Ag_2O) and CD90 (Ag_2O)). These catalysts were examined in catalytic actions for the degradation of MB, MO and EY dyes. Synthesized catalysts were also visualized for recycling turns in which catalysts showed encouraging results.

2. Experimental setup

2.1. Materials and methods

Sodium alginate (from brown algae, purity: 98%, CAS number: 9005-38-3, molecular weight: 405.2186 g/mol), chitosan (purity: 99%, ≥75% deacetylated, CAS number: 9012-76-4, molecular weight: 20,000 g/mol), Methylene blue (MB), Methyl orange (MO), Eosin Y (EY), acetic acid, sodium dodecyl sulfate (SDS), cetyltrimethylammonium bromide (CTAB), dimethylformamide, sodium borohydride ($NaBH_4$) and silver nitrate ($AgNO_3$) were purchased from Sigma-Aldrich (UK) and were used without further purification. Functionalized multi-walled carbon nanotubes (COOH-MWCNTs) were kindly provided by the National Center for Physics (NCP), Pakistan. Deionized water was used throughout the procedure.

2.2. Synthesis of silver oxide nanoparticles

Silver oxide metallic nanoparticles were prepared by following a reported method [30]. For such synthesis, a small amount of silver nitrate (170 mg) was dissolved in distilled water to form a dilute solution (0.001 M) by stirring. The aqueous solution of sodium borohydride (500 mL, 0.0020 M) was separately prepared by dissolving 0.378 mg of $NaBH_4$ in 500 mL of distilled water. Nanoparticles of silver oxide were prepared by stirring the ice-cold solution (30 mL) of sodium borohydride with the addition of silver nitrate (10 mL) dropwise (time interval between two drops should at least 10 s). The reaction mixture was filtered when it turned to darker yellow. Light brown precipitates of silver oxide were obtained on filter paper, washed several times with distilled water, and dried in 150°C for 6 h. These nanoparticles were sealed in vials and stored at room temperature for further use.

2.3. Synthesis of alginate-based catalysts

For the synthesis of alginate-based catalysts, a simple solution casting method was applied. A small quantity of alginate (0.9 g) was dissolved in deionized water (30 mL) by stirring at 40°C for 2 h. Functionalized COOH-MWCNTs

(0.016 g) were separately dissolved by sonication (2 h) in aqueous solution (30 mL) having a small amount of surfactants (SDS or CTAB) under ultrasonic waves produced by bath sonicator (Elmasonic S 30 H, 50–60 H). Chitosan (0.18 g) was dissolved in acetic acid solution (2%, 75 mL) by stirring at 30°C for 1 h. For the synthesis of alginate-based catalyst, a mixture solution of alginate (2 mL), COOH-MWCNTs (2 mL), chitosan (75 mL) and silver oxide nanoparticles (0.09 g) were further sonicated for 5 h at 40°C to obtain a homogeneous mixture. The obtained uniform blended mixture was poured into Petri plates and kept in a dust-free environment at room temperature for 3–4 weeks. Alginate-based nanocomposite films were washed with ethanol and dehydrated in the oven at 40°C for 5 h. Dried films were stored in sealed polyethylene bags for further processing.

In the solution mixture, when COOH-MWCNTs were dissolved in an aqueous solution having SDS as a surface acting agent than the formulated catalyst is coded as Cs90 (Ag_2O). When CTAB is used instead of SDS, then the catalyst is named as Cc90 (Ag_2O). And when no surfactant is used and COOH-MWCNTs are dispersed in the organic solvent then the obtained film is coded as CD90 (Ag_2O).

2.4. Characterization and measurements

Characterization and measurements of prepared silver oxide nanoparticles as well as of nanocomposites (catalysts) were done by using advanced instrumental techniques. Electronic transition in silver oxide particles was determined by UV-visible spectrophotometer (UV-1601 SHIMADZU, Korea) by dispersing the silver oxide particles in deionized water under ultrasonic waves. The nature of bonds and functional groups present in nanoparticles as well as in nanocomposites were identified by Fourier transform infrared spectroscopy (FTIR; PerkinElmer spectrum 100 series spectrometer, Korea) working in the range of 4,000–400 cm^{-1} at 2 mm/s rate. Surface study (morphology) of prepared materials was done by scanning electron microscopy (SEM; JEOL JSM-6510LV, 30 kV, Japan) technique working at 20 kV. The images were obtained at 300,000X (maximum magnification power) and 2.3 nm (maximum resolving power). Transmission electron microscopy (TEM) measurements were carried out on a JEOL JEM 1200 EXII (Japan) instrument operated at an accelerating voltage of 100.0 kV. The surface area of nanocomposites was determined by the Brunauer–Emmett–Teller (Quantachrome Nova 2200, USA) technique using ~0.045 g of the sample at 273 K. The shape, geometry, and pattern of arrangement in components were determined by X-rays diffractometry (XRD) technique using JDX-3532 diffractometer working at the voltage of 20–40 kV. The X-rays used were of 1.5418 Å to diffract the materials with a scanning range of 0°–160°.

2.5. Catalysis testing

Three types of prepared catalysts named Cs90 (Ag_2O), Cc90 (Ag_2O) and CD90 (Ag_2O) were explored for catalytic action in the degradation of three types of dyes (MB, MO and EY) by applying a reported method [31]. For such a study, a small piece (0.02 g) of the sample was immersed in a solution mixture (10 mL) formed by 100 mM of sodium borohydride (1 mL), 10^{-3} M of dye solution (1 mL), and 8 mL D.I water. This solution mixture was then stirred for a specific period until the dye is decolorized. Decolorized dye solution was filtered to remove catalysts and the extent of degradation was checked by taking UV absorbance. Each dye solution took different time for degradation in the presence of catalysts.

3. Results and discussions

3.1. Characterization and measurement of nanoparticles

The physical state and electronic position of prepared silver oxide nanoparticles are determined by UV-vis spectrophotometry (results are included in Fig. 1a). It is generally known that silver oxide particles absorb UV radiations in a 400–440 nm range [28]. The prepared brownish-black silver particles (image is displayed in Fig. 1a) showed a prominent absorption band with λ_{max} at 410 nm. This λ_{max} is attributed to surface plasmon resonance (SPR) that is created when light interacts with the surface of metallic oxide particles and consequently, collectively oscillation is produced in conduction electrons. Silver oxide nanoparticles have a unique optical property that is why the UV spectra provide a good deal related to physical states of metallic oxides. The appearance of broad band and shifting of SPR peak to longer wavelength indicates a bigger size and increased diameter of prepared nanoparticles. Similarly, a slightly secondary band appeared in the UV spectrum of as-grown particles are attributed to quadrupole resonance, which has a different electron oscillation than the primary dipole resonance. This appearance of the secondary band also indicates the anisotropy in particles.

As for non-spherical particles, the un-evenly distribution of surface plasmon resonance occurs, which leads to shape-dependent SPR absorption spectra [32]. According to Mie's theory, the shape of UV spectra in terms of the appearance of single or multiple bands is very crucial to estimate the geometry of particles. The particles that are spherical in nature always give a single band, whereas double or triple banded spectra are the indication of non-spherical geometry [33]. The appearance of multiple bands is attributed to plasma resonance or quadrupole or higher multiple plasmon excitation [33]. The obtained spectrum of as-grown silver oxide nanoparticles indicated that the particles are non-spherical in nature and have anisotropic geometry. Non-spherical shape of silver oxide particles is also indicated by SEM results.

The chemical nature and structural behavior of silver oxide particles were determined by FTIR spectroscopy at room temperature and shown by Fig. 1b. Prominent peaks related to various functional groups appeared at 3,487; 1,704; 1,450; 1,377; 1,232; 684 and 526 cm^{-1}. The peak appeared at 526 cm^{-1} is attributed to stretching vibration of Ag–O bond whereas, the absorption peak appeared at 684 cm^{-1} correspond to overtones produced by overlapping in stretching and bending vibrations of Ag–O bonds. The other stretching and bending absorptions appeared at various temperatures give an indication of the presence of some other materials along with silver oxide particles. It is known from various studies that at the time of

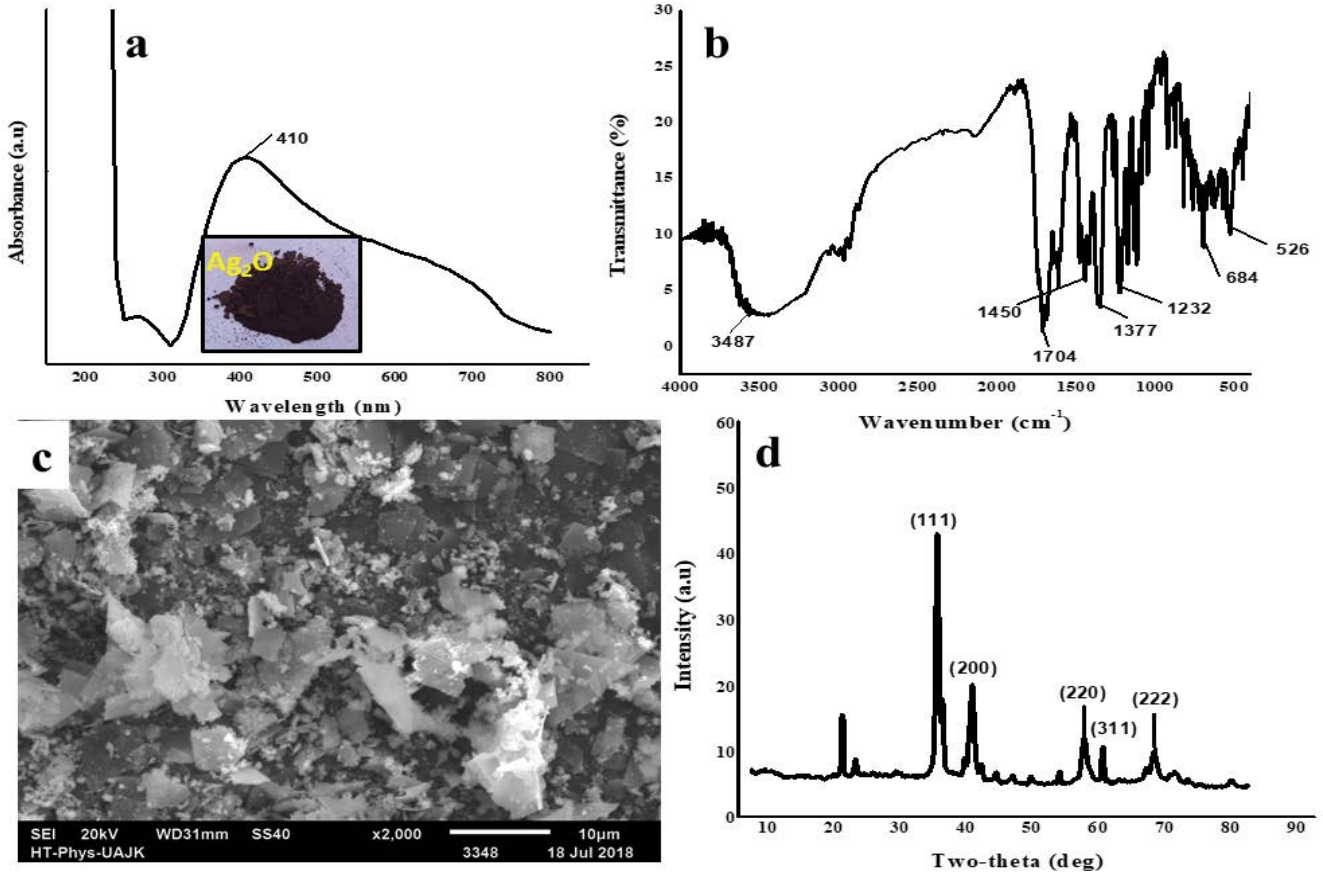

Fig. 1. (a) UV absorption spectrum of silver oxide particles, (b) FTIR spectrum of silver oxide particles, (c) SEM images of silver oxide particles and (d) XRD spectrum of silver oxide nanoparticles.

processing of silver oxide particles at room temperature, the upper surface is tarnished by CO_2 and atmospheric O_2 and some of the molecules of silver oxide are converted into Ag_2CO_3. In the presence of moisture, some of these Ag_2CO_3 molecules are converted into complex basic silver carbonate, having formula $AgOHAg_2CO_3$. From the spectral study of prepared nanoparticles, the possibility of formation of Ag_2CO_3 and complex $AgOHAg_2CO_3$ is obtained. The appearance of absorption peaks at various temperatures is the sign of υ_1, υ_2, υ_3 and υ_4 vibrations of carbonates and complex carbonates appeared at various energy bands [34,35]. The presence of the O–H group and C=O group along with the presence of Ag–O groups appeared at 3,478 and 1,704 cm^{-1} respectively. Similarly, the appearance of a doublet at 1,450 and 1,377 cm^{-1} is, in fact, the confirmation of conversion to basic silver carbonate [35].

The formation of somewhat complex silver compounds along with silver oxides is also indicated by SEM results. It is obtained that prepared nanoparticles have irregular geometry (shown in Fig. 1c). Some of the particles are in spheroidal shapes and some are anisotropic in nature with various particle sizes. This difference in geometry is due to the difference in oxidation states and the composition of silver oxide nanoparticles. It may be due to the formation of silver carbonate and complex basic silver carbonate along with silver oxide nanoparticles. The irregular geometry of particles is in accordance with another study [30]. The formation of such impurities is also indicated by those XRD peaks which were not consistent with a standard pattern. The SEM results further give an indication of the dispersed nature of prepared nanoparticles. Prepared materials are not present in agglomerated form but exist in somewhat scattered form. The pattern of dispersion is further enhanced on embedding in the polymeric matrix.

The structure and phase purity of synthesized nanoparticles were determined by XRD analysis. Fig. 1d represents the XRD pattern of prepared silver oxide nanoparticles. Diffraction peaks at 2θ = 32.95°, 38.30°, 55.18°, 65.64° and 69.07° can be indexed as (111), (200), (220), (311) and (222), respectively, correspond to the cubic structure of silver oxide (Ag_2O) matched with standard JCPDS No. 00-001-1041. The shapes of peaks indicate that highly pure and crystalline silver oxide particles are prepared. There are some peaks that appeared at 2θ = 18.6°, 20.6° and 58.0°. These values correspond to some impurities, it may be due to the presence of carbonates and complex basic carbonates which are formed by the interaction of silver oxide particles with atmospheric CO_2 and H_2O. The average crystallite size estimated with Scherrer's equation ($D = K\lambda/\beta \cos\theta$, where D = crystallite size, K = shape factor, λ = wavelength, β = full width at half maximum (FWHM) and θ = diffraction angle) from most intense peak along (111) plane was 28.85 nm.

3.2. Characterization and measurements of nanocomposites (catalysts)

Alginate-based nanocomposites having silver oxide nanoparticles along with COOH-MWCNTs are characterized by FTIR and results are included in Fig. 2a. The presence of each component in nanocomposite is represented by their respective absorption bands, for instance, the presence of the O–H bond in alginate and chitosan is confirmed by stretching vibration appeared at 3,460 cm^{-1}. Similarly, the presence of C=O conjugated with C=C bonds of COOH-MWCNTs is indicated by absorption peaks that appeared at 1,708 cm^{-1}. The C–O bonds present in carbohydrate rings of alginate and chitosan are indicated by stretching vibrations at 1,363 and 1,216 cm^{-1}. The presence of Ag–O bonds of silver oxide particles in nanocomposites is revealed by absorption peaks at 528 cm^{-1}. From this spectrum, it is indicated that during the processing, washing and drying process, the chemical composition of materials remained intact and nanoparticles did not agglomerate.

Dispersed nanoparticles entangle themselves and react with the polyelectrolytic complex of alginate–chitosan. The obtained blended scaffolds are amorphous in nature with some degree of crystallinity that is indicated by the XRD results (Fig. 2b). These crystallites may develop due to proper arrangements produced in polymeric chains. The sorts of interactions between nanofillers and polymers reduced segmental motion and arrayed the chains. The presence of crystallites is indicated by the presence of some small peaks obtained at about 2θ = 35.8°, 62.8°, 74.4°. On comparison of the peak pattern of nanocomposites with that of nanoparticles, the crystalline peaks of silver oxide disappeared in nanocomposite due to electrostatic interactions and H-bondings among alginate–chitosan, COOH-MWCNTs, and metallic oxide particles. The peaks obtained in nanocomposites are also less intense than silver oxide particles which are attributed to linkages present between components.

The surface morphology of catalysts was visualized by SEM analysis before and after the addition of silver oxide particles (results are included in Figs. 2c and d). On analysis, it is known that metallic oxide particles are uniformly dispersed and attached in a complex matrix of polymeric structures. Alginate is a negative polysaccharide while chitosan is a positive one, on suitable interaction, a strong polyelectrolytic complex is formed by embedding nanofillers (COOH-MWCNTs) under ultra-sonic waves. The polymeric structure obtained is very stable having plentiful reactive centers (–OH, –COOH and $–NH_2$ functional groups) and voids. On the addition of silver oxide particles in a polymeric matrix, reactive centers and cavities entrapped these particles thus porous scaffolds (catalysts) are formed. Nanofillers (COOH-MWCNTs) interacted with polymeric chains of alginate–chitosan matrix and provided a greater surface area to silver oxide particles by coordinating substrate molecules through noncovalent interactions. This dispersed and embedded nature of nanoparticles leads to the more stable, porous and active form of catalysts with

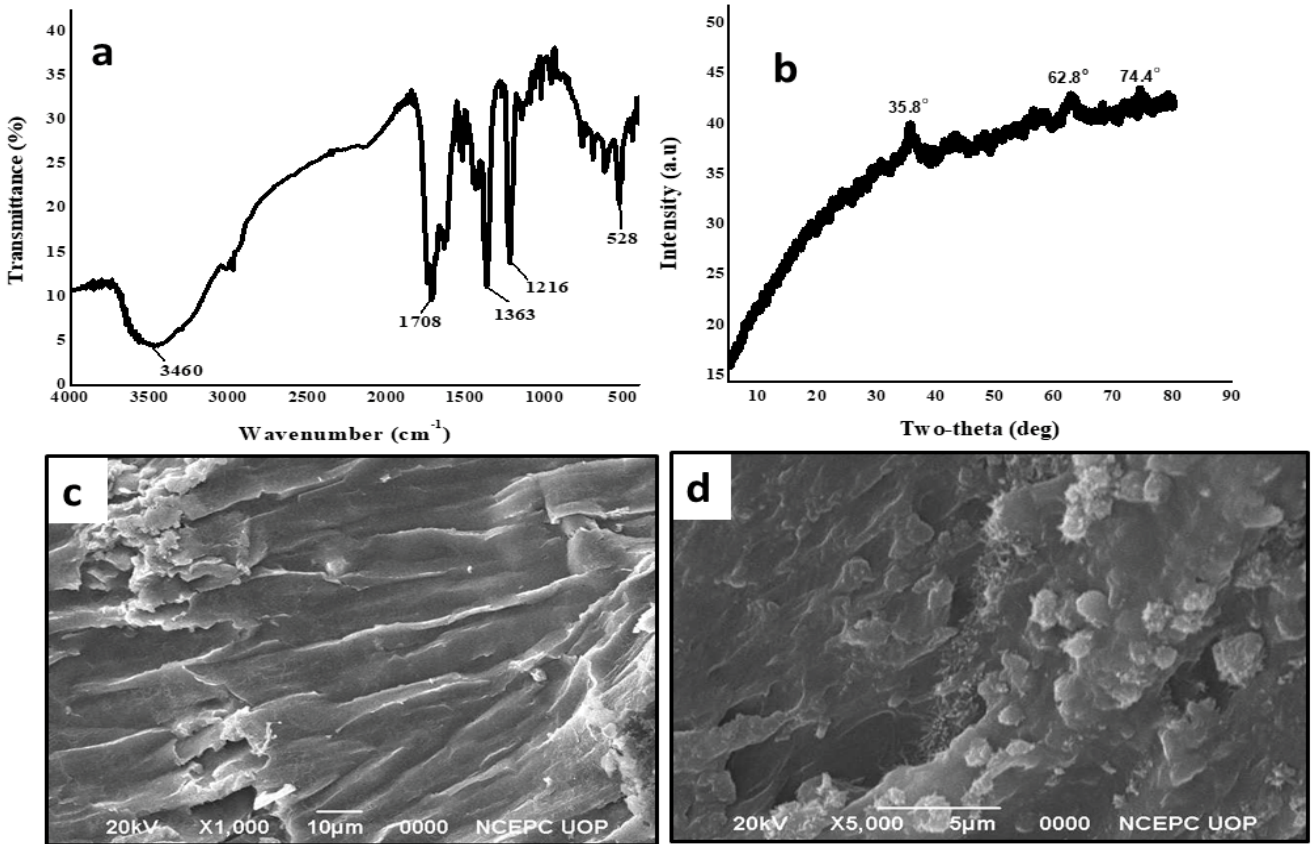

Fig. 2. (a) FTIR spectrum, (b) XRD spectrum and SEM images of (c) Cs90 nanocomposite and (d) Cs90 (Ag_2O) nanocomposites.

greater porosity. Bibi et al. [15] reported that there is a direct relationship between catalytic action and porosity. Our results related to the stable and cohesive nature of catalysts with leaching-less phenomenon even after washing, drying and formulation process are in accordance with the reported data [15].

On analysis of TEM results (shown in Figs. 3a–c), similar information related to the dispersed nature of nanofillers in the polymeric matrix was obtained. Alginate–chitosan interacts with each other in the presence of nanofillers; thus a very stable polyelectrolytic complex with more stability and water insolubility is formed. On the addition of silver oxide particles into this complex, attachment of silver oxide is obtained and formed the scaffolds with the greater surface area. The attachment of silver oxide particles in alginate-based nanocomposites is more favorable in the presence of MWCNTs (attachment is shown in Fig. 3c) and proposed structure of catalyst after embedding the silver oxide particles is represented by Fig. 3e.

From the SEM, TEM and XRD results, the various size distributions of nanoparticles are indicated. Size of particles are measured manually and found to be 30 ± 3, 38 ± 3, 54 ± 3 and 65 ± 3 nm with error range of about 3 nm. The relationship between peak intensity and size of particles is shown in Fig. 3d. It is indicated that the 30 ± 3 nm is the size of particles that are prepared with greater %. Fig. 1a also indicates that various sized particles are prepared and upon increasing the size, redshift in UV absorption was obtained with a broader band. The band becomes more significant when maximum size (65 ± 3) of particles is obtained. The XRD pattern (Fig. 1d) also confirms that there are five diffraction peaks lie between two theta 20° and 80° and are consistent with the peaks of all particle sizes.

To visualize the porosity of prepared catalysts, the surface area was determined before and after the addition of silver oxide particles (shown in Table 1). It is known that the surface area of nanocomposites is greater than the pristine polymers (alginate and chitosan). The inclusion of MWCNTs in the polyelectrolytic complex of alginate–chitosan matrix creates more pores with greater pore size and width. Moreover, the surface area of nanocomposites having surfactants is larger compared with non-surfactant containing nanocomposites. The higher value

Table 1
Surface area of synthesized nanocomposites (catalysts)

Types of samples	Specific surface area (m^2/g)	Pore volume (cm^3/g)	Pore width (nm)
Algi+chito	3.612	0.042	2.162
Cs90	8.436	0.007	3.179
Cc90	8.195	0.033	3.537
CD90	7.854	0.036	19.902
Cs90 (Ag_2O)	8.671	0.019	3.381
Cc90 (Ag_2O)	8.902	0.079	3.502
CD90 (Ag_2O)	7.893	0.026	16.997

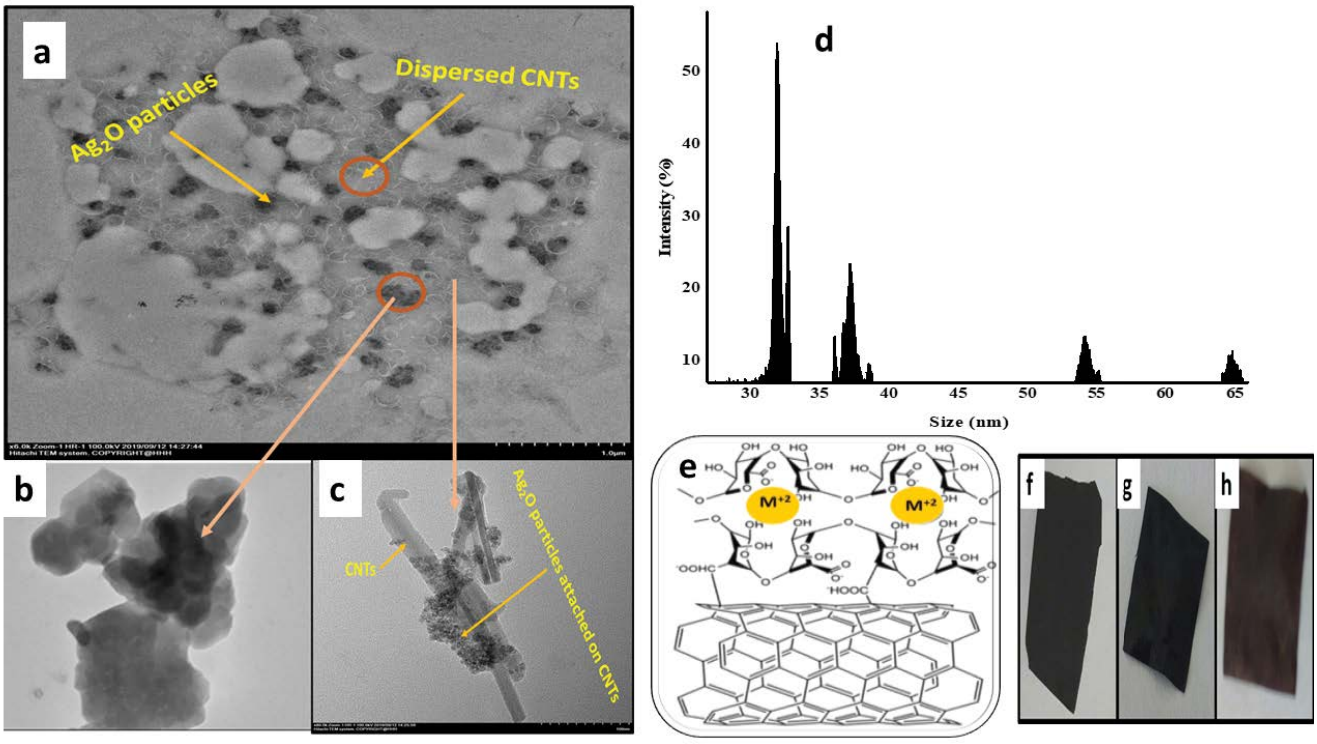

Fig. 3. TEM image of (a) nanocomposite, (b) MWCNTs having silver oxide nanoparticles, and (c) silver oxide particles, (d) particle size distribution of synthesized silver oxide nanoparticles, (e) interaction of CNTs with polymer matrix in the presence of metallic ions and (f–h) photographic images of synthesized Cc90 (Ag_2O), CD90 (Ag_2O), and Cs90 (Ag_2O) films.

in the presence of surfactants is attributed to the involvement of co-solutes in micelles formation around the outer ions. The greater porosity is responsible to diffuse more solvent into the films and greater is the rate of reaction. The porous nature of nanocomposite also provides greater reactive centers to reaction medium and speed up the reaction. It is obtained that on the addition of silver oxide particles into alginate–chitosan/CNTs nanocomposites, values of the surface area further increased. These increased values are explained based on the inclusion of metallic oxide particles in cavity formation. The porous nature of catalysts suggests the application of nanomaterials as the best candidate in the degradation of dyes.

3.3. Catalytic activity

3.3.1. Catalytic degradation of methylene blue

Methylene blue, a heterocyclic aromatic dye, is also called methylthioninium chloride is widely used in the textile industry for the time being. Methylene blue absorbs UV light at 662 nm (visible region), which is due to the π–π^* transition in dye molecules [31,36]. In order to know the extent of degradation of MB in the presence of synthesized catalysts, UV spectra were taken before and after the addition of catalysts. Initially, UV absorption of MB dye was measured in the presence of a reducing agent, that is, $NaBH_4$ without a catalyst. It is known that $NaBH_4$ is not largely affected in the degradation process as the absorption peak at 662 nm appeared with the persistence of blue color (shown in Fig. 4b). It may degrade the MB to some extent, but the degradation process was very low and seems to be non-considerable. However, when this reaction was repeated in the presence of catalysts (Cs90 (Ag_2O), Cc90 (Ag_2O), CD90 (Ag_2O)), rapid degradation of MB in 20–30 s was observed. This degradation process was confirmed by the disappearance of the absorption band at 662 nm and the decolorization of the MB solution. In fact, during the degradation process, MB is converted to leuco methylene blue (LMB), which is colorless in nature and inactive in the visible region [31]. In this catalytic reaction, silver oxide embedded in nanocomposite films accelerate the redox reaction between the donor ($NaBH_4$) and acceptor (MB) systems. Both these $NaBH_4$ and MB co-adsorb on the catalyst surface and enhance the relay of electrons between donor and acceptor, consequently degraded MB rapidly. On comparison of synthesized catalysts (nanocomposite films) with naked silver oxide particles, the efficiency of synthesized catalyst in the degradation of MB is 100 times more with much more regeneration potential. In the presence of naked silver oxide particles, MB is degraded in 20 min, but in our study, only a few seconds are required to complete the reaction [31]. The rapid degradation is assigned to more porous nature of films and dispersed form of silver oxide with more reactive centers, consequently, greater the possibility to react with dye molecules. Prepared catalysts were also comparatively analyzed with each other in the degradation reaction of MB. It is observed that Cs90 (Ag_2O) and Cc90 (Ag_2O) converted MB to LMB in 10–20 s, while in the presence of CD90 (Ag_2O), MB is degraded in about 35 min. The quick action of Cs90 (Ag_2O) and Cc90 (Ag_2O is ascertained to the presence of surfactants (SDS and CTAB, respectively). In the presence of surfactants, micelles are formed around the metallic particles by electrostatic and non-electrostatic types of interactions and keep the metallic particles in the dispersed form [37]. Furthermore, surfactants also facilitate the rate of diffusion of solvent in films due to greater solubility and catalytic action becomes rapidly. The complete mechanism involved in catalysis in the presence of surfactants is not fully understood, perhaps it may be the dissolution of the surface layer of micelles and exposure of metallic oxide

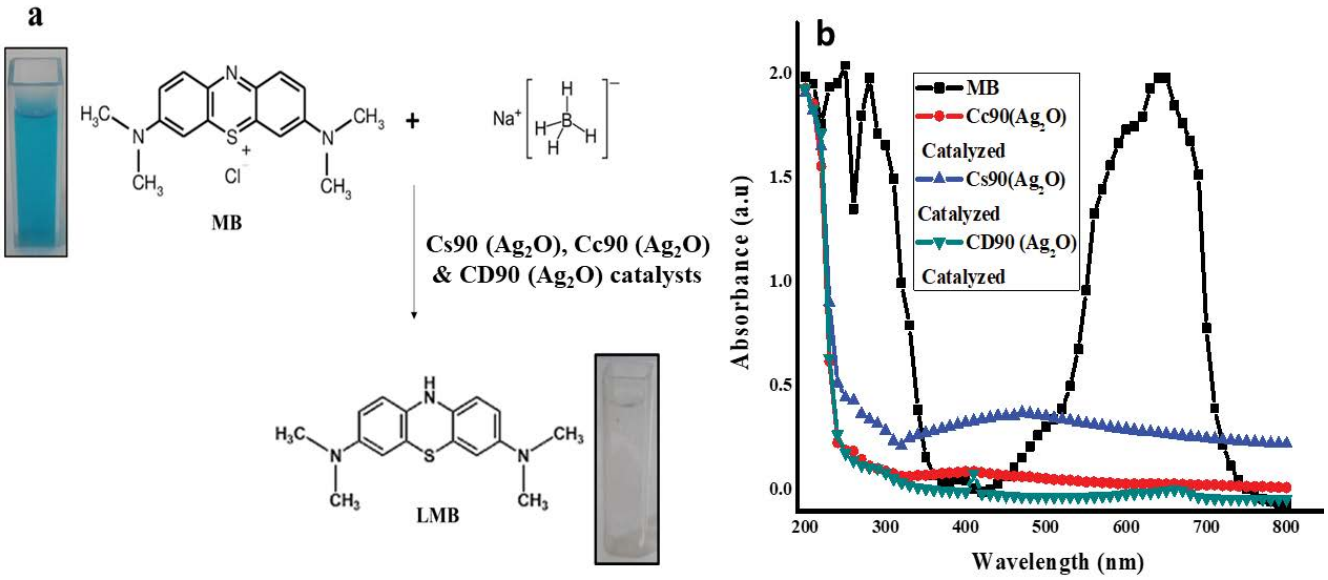

Fig. 4. (a) Reaction pathway for conversion of MB to LMB in the presence of synthesized catalysts and (b) UV absorption spectra of catalyzed and un-catalyzed MB.

particles (provide more reactive centers), which react fully with dye molecules and degrade it. While in CD90 (Ag_2O), there was a significant induction period before the reaction commenced, presumably due to the time required for penetration in films and start the catalytic action. That is why the time required to catalyze the MB is prolonged (i.e., 35 min). The reaction pathway in which MB is converted into LMB is shown by the schematic diagram (Fig. 4a).

3.3.2. Catalytic degradation of methyl orange

Methyl orange is a sulfosalt and by nature, it is an organic dye. This dye is continuously added to water bodies and is very harmful to human and aquatic life. In the presence of UV light, MO absorbs at 465 nm. In the current study, first of all, the degradation process of MO was evaluated in the presence of a reducing agent, which is $NaBH_4$. It is observed that in the presence of this reducing agent, MO is not degraded and gives the absorption band at 465 nm as usual (shown in Fig. 5b). Perhaps, it may be degraded, but it was very low to show its effect at room temperature. However, when the solution of MO was degraded in the presence of $NaBH_4$ and catalysts, the reaction of degradation proceeded very rapidly. It is estimated that, in the presence of catalysts (Cs90 (Ag_2O), Cc90 (Ag_2O), and CD90 (Ag_2O)) and reducing agent, MO is converted into small non-toxic hydrazine in limited time. This catalytic action is confirmed by the disappearance of the absorption band at 465 nm and appearance of a new absorption peak at 250 nm. The mechanism involved in this process is a simple oxidation–reduction mechanism, in which electrons are donated by $NaBH_4$ and accepted by MO. However, in normal conditions, this electron array is not feasible without a catalyst. Catalysts co-adsorb the electron donor and acceptor on their surface and enhance the degradation process by electron transfer process. The comparative study of catalysts indicated the high efficiency of Cc90 (Ag_2O) and Cs90 (Ag_2O) compared with CD90 (Ag_2O). Due to the soluble nature of surfactants and greater surface area, silver oxide particles were exposed more in aqueous solution and catalyzed MO in 13–15 min. However, CD90 (Ag_2O) required a longer time (~ 1 h) to catalyze the MO into hydrazine. The synthesized catalysts were also tested for their efficiency with pristine silver oxide particles in the degradation of MO [31]. There was no distinct difference observed, as pristine silver oxide particles took almost similar time to degrade the MO. However, the superiority of newly prepared catalysts is the regeneration and extended recycling turns (11 times) with no loss in mass. The reaction pathway for conversion of MO to hydrazine is shown in Fig. 5a.

3.3.3. Catalytic degradation of eosin Y

Eosin Y is an organic dye and is also called tetrabromofluorescein. This dye gives an intense pink-orange (abbey) color on solubilizing in water. It is largely used in paper, pulp and textile industry [38]. The degradation reaction of Eosin Y was studied before and after the addition of catalysts. First, the UV absorption of the Eosin Y solution was measured in the presence of reducing agent $NaBH_4$. It is known that an absorption band at 520 nm was observed, which the characteristics lambda max is for Eosin Y (Fig. 6b). When the catalyst was added in the dye solution along with reducing agent, degradation reaction occurred in which orange color is converted into a yellowish-green color. The confirmation of degradation reaction was done by UV absorption bands of catalyzed dye. In these absorption bands, degradation reaction is indicated by the disappearance of the absorption band from 520 nm. The mechanism involved in this degradation is also an oxidation–reduction reaction similar to MB and MO. In this redox reaction, one electron is transferred and the orange color of eosin (ES_2^-) is converted into yellowish-green (ES_2H) [39]. This transferring of electrons is facilitated using catalysts, which speed up the reaction and hence the degradation reaction is completed in 20–25 min. Synthesized catalysts were compared with each other based on efficiency and found that surfactants containing catalysts showed the best performance compared with non-surfactant containing film. Again, the larger surface area and the role of surfactants in

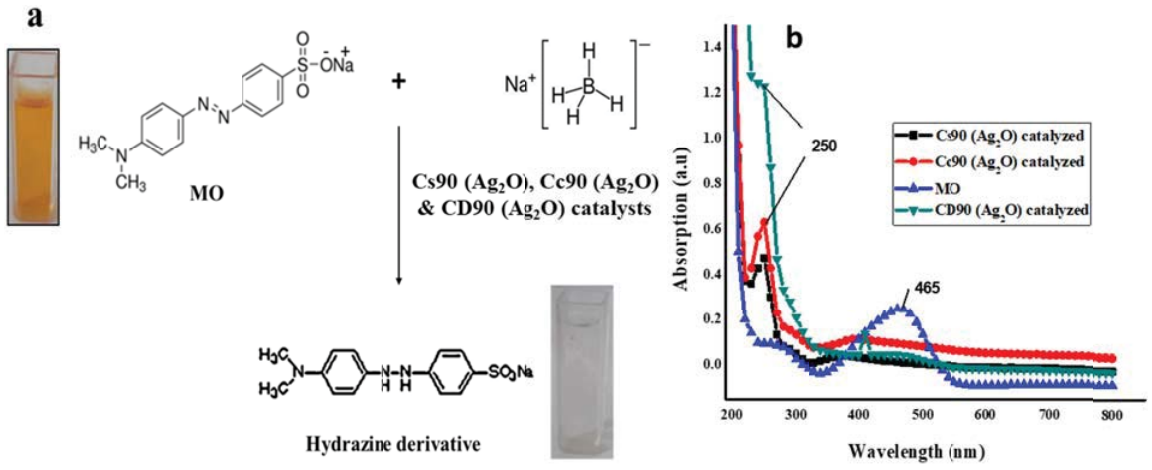

Fig. 5. (a) Reaction pathway for conversion of MO into hydrazine derivative in the presence of synthesized catalysts and (b) UV absorption spectra of catalyzed and un-catalyzed MO.

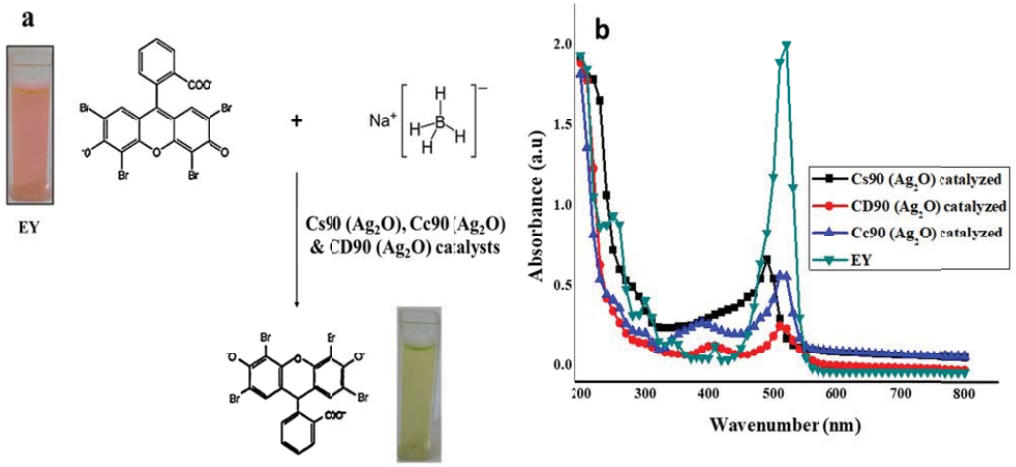

Fig. 6. (a) Reaction pathway for degradation of Eosin Y in the presence of synthesized catalysts, and (b) UV absorption spectra of catalyzed and un-catalyzed Eosin EY.

exposing the nanoparticles in aqueous media is the reason for quick action. While in CD90 (Ag_2O), no such co-solutes are involved and hence more time (~1 h) is required to complete the degradation process. More stability of catalysts and quick action as compared with pristine silver nanoparticles recommend that nanocomposite films containing silver oxide particles can act as the best catalysts for degradation of three types of dyes namely MB, MO and EY. The type of reaction involved in the degradation reaction of EY is illustrated by an equation in Fig. 6a.

3.3.4. Mechanism of catalytic degradation

The catalytic action of synthesized catalysts is studied in the presence of $NaBH_4$. It is investigated from the reported data that the understudy dyes were degraded in the presence of reducing agent, that is, $NaBH_4$, but in a very small amount. However, when the small piece of catalyst is added along with $NaBH_4$, the degradation reaction is accelerated, and dyes are catalyzed within seconds. This rapid action is due to the oxidation–reduction reaction occurring between the donor ($NaBH_4$) and acceptor (dye) molecules. $NaBH_4$ molecules dissolve in water and liberate one H^- atom (shown in the following equation) [40].

$$BH_4^- \rightleftarrows BH_3 + H^- \quad (1)$$

$$2H^- \rightleftarrows H_2 + 2e^- \quad (2)$$

The two H^- atoms react with each other and two electrons are released. The silver oxide embedded catalysts (nanomaterials) act as electron acceptor/donor and relay the electrons to the organic dye, thus degraded it. In the catalysts, this array of electrons is transferred from the valence band to the conduction band, where they are removed by the oxygen dissolved in water and converted into $^{\bullet}O_2^-$. The hole in the valence band reacts with OH^- of water to form hydroxyl radical $^{\bullet}OH$ [41]. The scheme of degradation is shown in the following figure (Fig. 7).

As a result of these reactions, the nascent hydroxyl radicle and oxygen radical act as highly oxidizing agents, which react with dyes and convert them into simple and less toxic substances. The small degraded products are very often unstable and easily degraded into simpler products.

For instance, upon catalytic degradation, MB is converted into LMB, which is a colorless compound. It is highly unstable in its solid form and is sensitive to dioxygen. It reacts with oxygen and breaks down into smaller components that are less toxic compared with azo dyes such as MB. That is why on the industrial scale, efforts are carried out to find a useful technology for the degradation reaction of MB.

Similarly, the cationic form of MO is very susceptible to free electrons; on reacting with electrons, it is degraded and gets converted into hydrazine derivative, which is unstable in solid form and is converted into hydrazone and hydrazide products. On complete oxidation, hydrazine is converted into water and nitrogen; on partial oxidation, it is converted into nitrogen and ammonia. Thus, degradation products of methyl orange are less toxic and environmentally benign.

Eosin Y exists in a cationic form in aqueous solution; on accepting the electrons, it is degraded and gets converted into a less toxic substance, which is further degraded into CO_2 and H_2O. These results convince us to conclude that catalytic degradation is a remedy technology to reduce the water pollution caused by aromatic, stable and toxic organic dyes.

3.3.5. Recycling of catalysts in the degradation of dyes

The long-term reusability and stability are important parameters for a catalyst to be used in an industry. As a preliminary exploration, we used our catalysts for a number of times in the degradation of MB, MO and Eosin Y. The recycling turns in which catalysts are successfully applied are shown in Table 2.

In each reaction cycle, catalysts were washed 3–4 times with distilled water and introduced into a new bath of reactants. It was obtained that the catalysts Cs90 (Ag_2O) and

Table 2
Recycling turns in which synthesized films are used for the catalytic action of dyes

S. No	Types of films	Recycling turns for degradation of dyes		
		MB	MO	EY
1	Cs90 (Ag_2O)	23	11	7
2	Cc90 (Ag_2O)	23	11	7
3	CD90 (Ag_2O)	10	6	4

Cc90 (Ag_2O) were successfully applied to degrade the MB dye for 23 times. After the 23rd cycle, catalyst retained their action in the reaction bath, but after removing them, slightly bluish color regenerated, suggesting incomplete degradation. While CD90 (Ag_2O) catalyst can catalyze the reaction successfully for 10 times. To enhance further catalytic action of prepared catalysts after using such repeated time, films can be treated with other methods (with acid, sonication or other ways) for activeness. It was found that even after using the catalysts for such prolonged times (23rd cycle), the cohesiveness, strength and shape of catalysts remained intact. Such type of mechanical stability gives an indication of strong interaction between polymeric materials and nanofillers. The time required for each degraded reaction did not vary more than a few minutes. Initially, MB dye was converted into LMB in just 20–30 s but last (23rd) recycling reaction was completed in 6 min. The delayed time required in the last recycling use is attributed to the least availability of dye-loaded reactive centers for degradation of MB, indicating the saturation of catalytic surface with dye molecules. Actually, it is associated with incomplete removal of bound dye molecules from the surface of catalysts that decay the catalytically active sites. These results confirm the strong immobilization and well dispersion of silver oxide particles indicating that the leaching out process has not occurred.

In the same way, the synthesized catalysts were applied for the repeated catalytic reaction of MO. It was found that Cs90 (Ag_2O) and Cc90 (Ag_2O) are recycled very efficiently for 11 times, while CD90 (Ag_2O) is recycled for 6 times. After that recycling turns, catalysts remain intact, but they required a long time to complete the reaction.

Likewise, the catalytic conversion process of EY dye was recycled seven times. Experiments revealed that Cc90 (Ag_2O) and Cs90 (Ag_2O) catalysts showed the best activity in recycling reaction (7 times). Prepared film CD90 (Ag_2O) degraded the EY dye for four times. The time required for each recycled process did not vary

Table 3
Comparison of degradation reaction of synthesized catalysts with reported catalysts

S. No	Catalysts	Dye degraded	Recycling turn	References
1	Silver metal dispersed in 2-acrylamido-2-methylpropane sulfonate-co-vinylpyrrolidone matrix	Methylene blue (MB)	8 times	43
2	TiO_2/Ag metal deposited on quartz substrate	Methylene blue (MB)	1 time	44
3	TiO_2 embedded in ca-alginate support	Methylene blue (MB)	3 times	10
4	Ag/Pt particles decorated on Si substrates	Methyl orange (MO)	4 times	45
5	Ag-doped Fe_3O_4 nanomaterials	Eosin Y (EY)	3 times	46
6	Ag_2O embedded in Alginate–chitosan/MWCNTs support	MB MO EY	23 times 11 times 7 times	This work

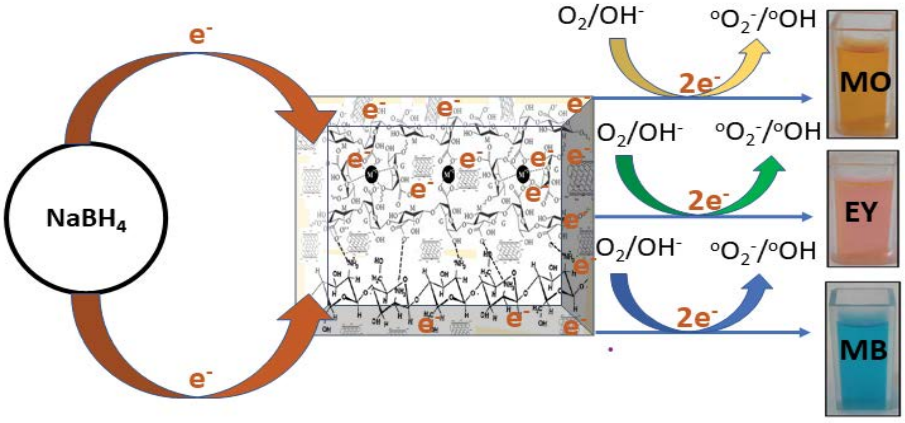

Fig. 7. Degradation mechanism of organic dyes in the presence of synthesized catalysts.

more than minutes and catalysts successfully degraded seven times.

In the field of catalysis, the recovery of catalysts is difficult and is the main issue. Most of the catalysts employed are converted into colloidal form and they were recovered by centrifugation process, which is a difficult process [42]. Now, it is a growing trend to use support for stabilizing the catalysts. Supports not only provide the catalysts with large reacting sites but also prevent from leaching process. Therefore, we prepared catalysts embedded in support and found the best results in catalytic action.

From this study, it is concluded that prepared nanocomposites are appropriate for direct inclusion in a flow system. These catalysts can be employed in a filter bed or in the lining of the reactor. These catalysts would be efficient for an extended period and recovery problems would be negligible.

3.3.6. Comparison of catalytic degradation with other studies

The catalytic action of synthesized catalysts is compared with other matrix-embedded catalysts [10,43–46] listed in Table 3. The proposed nanostructure of prepared catalysts is comparable and competitive with other studies. The rapid catalytic action and subsequent regenerative cycles make the prepared catalysts as most promising from a cost-effectiveness point of view. Other silver-containing supporting materials also showed the best catalytic action in the degradation of organic dyes, but these are less efficient compared to synthesized catalysts. Moreover, synthesized catalysts showed greater regenerative cycles due to internal cohesiveness and reactive centers. In the current study, catalysts degraded the MB, MO and EY for 23, 11 and 7 times, respectively. This behavior is due to the presence of reactive centers on the surface of catalysts created by COOH-CNTs and the polymeric matrix. Additionally, greater porosity, nano size of reinforcing particles, and possibly greater interaction between the components make the catalysts as more stable and efficient with variable voids and channels. The molecules of dye react physio-chemically with reactive centers of catalysts and get degraded into smaller less-toxic components.

4. Conclusion

Prepared nanocomposites having embedded metallic particles acted as the best catalysts due to the dispersed metallic oxide particles, greater reactive centers, and immobilized nature. There is a strong interaction that occurred in nanoparticles and supporting matrix. These types of interactions result in creating cohesiveness and stability in prepared nanocomposites. Three dyes namely MB, MO and EY were successfully degraded by synthesized catalysts in no time. The MB was degraded in 20–30 s, MO in 30–35 min, and EY in 20–25 min. The role of surfactants in quick catalytic action was appreciated by providing more solubility, surface area, and reactive centers for degradation. Synthesized catalysts have the potential to be used in many recycling turns. For instance, Cs90 (Ag_2O) and Cc90 (Ag_2O) degraded MB for 23 times, MO for 11 times and EY 7 times successfully. Compared with their counterparts pristine particles and other matrix-based catalysts, nanocomposite catalysts are considered to be more efficient. This study recommends the application of these novel catalysts in different places such as the lining of the reactor, filter-bed or in flow-system.

Acknowledgments

The authors are grateful to the National Center for Physics, Pakistan, for kindly providing MWCNTs. The authors are also thankful to Dr. Muhammad Farooq, UOP Pakistan, and Mr. Bilal Akram, Tsinghua University, China, for their help in characterizing the samples.

References

[1] Z. Hasan, S.H. Jhung, Removal of hazardous organics from water using metal-organic frameworks (MOFs): plausible mechanisms for selective adsorptions, J. Hazard. Mater., 283 (2015) 329–339.
[2] J. Abdi, M. Vossoughi, N.M. Mahmoodi, I. Alemzadeh, Synthesis of amine-modified Zeolitic imidazolate framework-8, ultrasound-assisted dye removal, and modeling, Ultrason. Sonochem., 39 (2017) 550–564.
[3] Hazardous Substance Research Centers/South and Southwest Outreach Program (2005) Environmental Hazards of the Textile Industry. Environmental Update #24, Business Week [Citation Time(s):2].
[4] M.A. Kamal, S. Bibi, S.W. Bokhari, A.H. Siddique, T. Yasin, Synthesis and adsorptive characteristics of novel chitosan/graphene oxide nanocomposite for dye uptake, React. Funct. Polym., 110 (2017) 21–29.
[5] S. Ghorai, A.K. Sarkar, A.B. Panda, S. Pal, Effective removal of Congo red dye from aqueous solution using modified xanthan gum/silica hybrid nanocomposite as adsorbent, Bioresour. Technol., 144 (2013) 485–491.
[6] B.C. Ventura-Camargo, M.A. Marin-Morales, Azo dyes: characterization and toxicity-a review, Text. Light Ind. Sci. Technol., 2 (2013) 86–103.
[7] R. Kant, Textile dyeing industry an environmental hazard, Nat. Sci., 4 (2012) 22–26.
[8] J. Abdi, M. Vossoughi, N. Mohammad Mahmoodi, I. Alemzadeh, Synthesis of metalorganic framework hybrid nanocomposites based on GO and CNT with high adsorption capacity for dye removal, Chem. Eng. J., 326 (2017) 1145–1158,
[9] D.T. Santos, B.F. Sarrouh, J.D. Rivaldia, A. Converti, S.S. Silva, Use of sugarcane bagasse as a biomaterial for cell immobilization for xylitol production, J. Food Eng., 86 (2008) 542–548.
[10] J.Q. Albarelli, D.T. Santos, S. Murphy, M. Oelgemöller, Use of Ca-alginate as a novel support for TiO_2 immobilization in methylene blue decolorization, Water Sci. Technol., 60 (2009) 1081–1087.
[11] K. Thirumalai, S. Balachandran, M. Swaminathan, Superior photocatalytic, electrocatalytic, and self-cleaning applications of Fly ash supported ZnO nanorods, Mater. Chem. Phys., 183 (2016) 191–200.
[12] K. Selvakumar, A. Raja, M. Arunpandian, K. Stalindurai, P. Rajasekaran, P. Sami, E.R. Nagarajan, M. Swaminathan, Efficient photocatalytic degradation of ciprofloxacin and bisphenol a under visible light using Gd_2WO_6 loaded ZnO/bentonite nanocomposites, Appl. Surf. Sci., 481 (2019) 1109–1119.
[13] K. Thirumalai, E.T.D. Kumar, R. Aravindhan, J.R. Rao, M. Swaminathan, Hierarchically structured bentonite loaded Bi_2O_3-ZnO and its multiple applications, Surf. Interfaces, 5 (2016) 30–38.
[14] D.P. Stankus, S.E. Lohse, J.E. Hutchison, J.A. Nason, Interactions between natural organic matter and gold nanoparticles stabilized with different organic capping agents, Environ. Sci. Technol., 45 (2011) 3238–3244.

[15] S. Bibi, G.J. Price, T. Yasin, M. Nawaz, Eco-friendly synthesis and catalytic application of chitosan/gold/carbon nanotube nanocomposite films, RSC Adv., 6 (2016) 60180–60186.
[16] E. Guibal, Heterogeneous catalysis on chitosan-based materials: a review, Prog. Polym. Sci., 30 (2005) 71–109.
[17] H. Huang, X. Yang, Synthesis of chitosan-stabilized gold nanoparticles in the absence/presence of tripolyphosphate, Biomacromolecules, 5 (2004) 2340–2346.
[18] K. Norajit, K.M. Kim, G.H. Ryu, Comparative studies on the characterization and antioxidant properties of biodegradable alginate films containing ginseng extract, J. Food Eng., 98 (2010) 377–384.
[19] C. Jouannin, C. Vincent, I. Dez, A.C. Gaumont, T. Vincent, E. Guibal, Study of alginate-supported ionic liquid and Pd catalysts, Nanomaterials, 2 (2012) 31–53.
[20] M. Zeng, X. Yuan, Z. Yang, C. Qi, Novel macroporous palladium cation crosslinked chitosan membranes for heterogeneous catalysis application, Int. J. Biol. Macromol., 68 (2014) 189–197.
[21] A. Bibi, Sadiq-ur-Rehman, A. Yaseen, Alginate-nanoparticles composites: kinds, reactions and applications, Mater. Res. Express, 6 (2019) 092001.
[22] A. Bibi, Sadiq-ur-Rehman, R. Fiaz, T. Akhtar, M. Nawaz, S. Bibi, Effect of surfactants on swelling capacity and kinetics of alginate-chitosan/CNTs hydrogel, Mater. Res. Express, 6 (2019) 085065.
[23] G.J. Price, M. Nawaz, T. Yasin, S. Bibi, Sonochemical modification of carbon nanotubes for enhanced nanocomposite performance, Ultrason. Sonochem., 40 (2018) 123–130.
[24] M. Arjmand, K. Chizari, B. Krause, P. Pötschke, U. Sundararaj, Effect of synthesis catalyst on the structure of nitrogen-doped carbon nanotubes and electrical conductivity and electromagnetic interference shielding of their polymeric nanocomposites, Carbon, 98 (2016) 358–372.
[25] B. Galindo, A. Benedito, E. Gimenez, V. Compañ, Comparative study between the microwave heating efficiency of carbon nanotubes versus multilayer graphene in polypropylene nanocomposites, Compos. Part B Eng., 98 (2016) 330–338.
[26] X. Wu, C. Lu, Y. Han, Z. Zhou, G. Yuan, X. Zhang, Cellulose nanowhisker modulated 3D the hierarchical conductive structure of carbon black/natural rubber nanocomposites for liquid and strain sensing applications, Compos. Sci. Technol., 124 (2016) 44–51.
[27] F. Karkeh-Abadi, S. Saber-Samandari, S. Saber-Samandari, The impact of functionalized CNT in the network of sodium alginate-based nanocomposite beads on the removal of Co(II) ions from aqueous solutions, J. Hazard. Mater., 312 (2016) 224–233.
[28] L. Ai, M. Li, L. Li, Adsorption of methylene blue from aqueous solution with activated carbon/cobalt ferrite/alginate composite beads: kinetics, isotherms, and thermodynamics, J. Chem. Eng. Data, 56 (2011) 3475–3483.
[29] M. Ionita, M.A. Pandele, H. Iovu, Sodium alginate/graphene oxide composite films with enhanced thermal and mechanical properties, Carbohydr. Polym., 94 (2013) 339–344.
[30] U.T. Khatoon, K.V. Rao, J.V.R. Rao, Y. Aparna, Synthesis, and Characterization of Silver Nanoparticles by Chemical Reduction Method, International Conference on Nanoscience, Engineering and Technology (ICNET), 228–30 Nov. 2011, Chennai, India, 2011.
[31] V.K. Vidhu, D. Philip, Catalytic degradation of organic dyes using biosynthesized silver nanoparticles, Micron, 56 (2014) 54–62.
[32] Y.G. Sun, Y.N. Xia, Plasmonics: Metallic Nanostructures and Their Optical Properties, Proceedings of SPIE, Vol. 5221, 2003, pp. 170–173.
[33] G. Mie, Contributions to the optics of turbid media, particularly of colloidal metal solutions, Ann. Phys., 25 (1908) 377–445.
[34] B.M. Gatehouse, S.E. Livingstone, R.S. Nyholm, The infrared spectra of some simple and complex carbonates, J. Chem. Soc., 3 (1958) 1–37.
[35] T.L. Slager, B.J. Lindgren, A.J. Mallmann, R.G. Greenler, Infrared spectra of the oxides and carbonates of silver, J. Phys. Chem., 76 (1972) 940–943.
[36] T. Shahwan, S.A. Sirriah, M. Nairat, E. Boyac, A.E. Eroglu, T.B. Scott, K.R. Hallam, Green synthesis of iron nanoparticles and their application as a Fenton-like catalyst for the degradation of aqueous cationic and anionic dyes, Chem. Eng. J., 172 (2011) 258–266.
[37] J. Hedberg, M. Lundin, T. Lowe, E. Blomberg, S. Wold, I.O. Wallinder, Interactions between surfactants and silver nanoparticles of varying charges, J. Colloid Interface Sci., 369 (2012) 193–201.
[38] K. Vignesh, R. Priyanka, R. Hariharan, M. Rajarajan, A. Suganthi, Fabrication of CdS and $CuWO_4$ modified TiO_2 nanoparticles and their photocatalytic activity under visible light Irradiation, J. Ind. Eng. Chem., 20 (2014) 435–443.
[39] J. Santhanalakshmi, P. Venkatesan, Mono and bimetallic nanoparticles of gold, silver and palladium-catalyzed NADH oxidation-coupled reduction of eosin-Y, J. Nanopart. Res., 13 (2011) 479–490.
[40] Z.C. Kadirovaa, K. Katsumata, T. Isobec, N. Matsushita, A. Naka-jima, K. Okada, Adsorption and photodegradation of methylene blue by iron oxide impregnated on granular activated carbons in an oxalate solution, Appl. Surf. Sci., 284 (2013) 72–79.
[41] Y.H. Chiu, T.F.M. Chang, C.Y. Chen, M. Sone, Y.J. Hsu, Mechanistic insights into photodegradation of organic dyes using heterostructure photocatalysts, Catalysts, 9 (2019) 430.
[42] R. Rajesh, E. Sujanthi, S.S. Kumar, R. Venkatesan, designing versatile heterogeneous catalysts based on Ag and Au nanoparticles decorated on chitosan functionalized graphene oxide, Phys. Chem. Chem. Phys., 17 (2015) 11329–11340.
[43] A.M. Atta, Y.M. Moustafa, H.A. Al-Lohedan, A.O, Ezzat, A.I. Hashem, Methylene Blue catalytic degradation using silver and magnetite nanoparticles functionalized with a poly (ionic liquid) based on quaternized dialkylethanolamine with 2-acrylamido-2-methylpropane sulfonate-co-vinylpyrrolidone, ACS Omega, 5 (2020) 2829–2842.
[44] P. Sangpour, F. Hashemi, A.Z. Moshfegh, Photoenhanced degradation of methylene blue on cosputtered M:TiO_2 (M = Au, Ag, Cu) nanocomposite systems: a comparative study, J. Phys. Chem. C, 114 (2010) 13955–13961.
[45] M. Sakir, M.S. Onses, Solid substrates decorated with Ag nanostructures for the catalytic degradation of methyl orange, Results Phys., 12 (2019) 1133–1141.
[46] E. Alzahrani, Photodegradation of eosin Y using silver-doped magnetic nanoparticles, Int. J. Anal. Chem., 2015 (2015) 1–11.